Published in final edited form as:
Cancer Res. 2010 May 1; 70(9): 3687–3696. doi:10.1158/0008-5472.CAN-09-3931.

Sustained Small Interfering RNA Delivery by Mesoporous Silicon Particles

Takemi Tanaka[1,9], **Lingegowda S. Mangala**[2], **Pablo E. Vivas-Mejia**[11], **René Nieves-Alicea**[1], **Aman P. Mann**[1], **Edna Mora**[2,5,10,11], **Hee-Dong Han**[2], **Mian M.K. Shahzad**[2,8], **Xuewu Liu**[1,9], **Rohan Bhavane**[1], **Jianhua Gu**[1], **Jean R. Fakhoury**[1,9], **Ciro Chiappini**[9], **Chunhua Lu**[2], **Koji Matsuo**[2], **Biana Godin**[1], **Rebecca L. Stone**[2], **Alpa M. Nick**[2], **Gabriel Lopez-Berestein**[3,4,6], **Anil K. Sood**[2,3,6], and **Mauro Ferrari**[1,4,6,7,9]

[1]Department of Nanomedicine and Biomedical Engineering, University of Texas Health Science Center at Houston, Houston, Texas

[2]Department of Gynecologic Oncology, University of Texas M.D. Anderson Cancer Center, Houston, Texas

[3]Department of Cancer Biology, University of Texas M.D. Anderson Cancer Center, Houston, Texas

[4]Department of Experimental Therapeutics, University of Texas M.D. Anderson Cancer Center, Houston, Texas

[5]Department of Surgical Oncology, University of Texas M.D. Anderson Cancer Center, Houston, Texas

[6]Center for RNA Interference and Non-Coding RNA, University of Texas M.D. Anderson Cancer Center, Houston, Texas

[7]Department of Bioengineering, Rice University, Houston, Texas

[8]Department of Obstetrics and Gynecology, Baylor College of Medicine, Houston, Texas

[9]Department of Biomedical Engineering, University of Texas Austin, Austin, Texas

[10]Department of Surgery, San Juan, Puerto Rico

[11]The University of Puerto Rico Comprehensive Cancer Center, San Juan, Puerto Rico

Abstract

RNA interference (RNAi) is a powerful approach for silencing genes associated with a variety of pathologic conditions; however, *in vivo* RNAi delivery has remained a major challenge due to lack of safe, efficient, and sustained systemic delivery. Here, we report on a novel approach to overcome these limitations using a multistage vector composed of mesoporous silicon particles (stage 1 microparticles, S1MP) loaded with neutral nanoliposomes (dioleoyl phosphatidylcholine, DOPC) containing small interfering RNA (siRNA) targeted against the EphA2 oncoprotein, which

Corresponding Author: Mauro Ferrari, The University of Texas Health Science Center, 1825 Pressler Street, Houston, TX 77030. Phone: 713-500-2470; Fax: 713-500-2462; Mauro.Ferrari@uth.tmc.edu.
T. Tanaka and L.S. Mangala contributed equally to this work.

Note: Supplementary data for this article are available at Cancer Research Online (http://cancerres.aacrjournals.org/).

Disclosure of Potential Conflicts of Interest

Commercialization rights on the intellectual property presented in this article have been acquired by Leonardo Biosystems Inc. from the title holder, the University of Texas Health Science Center in Houston. M. Ferrari is the founding scientist of Leonardo Biosystems, and hereby discloses a financial interest in the company. The other authors disclosed no potential conflicts of interest.

is overexpressed in most cancers, including ovarian. Our delivery methods resulted in sustained EphA2 gene silencing for at least 3 weeks in two independent orthotopic mouse models of ovarian cancer following a single i.v. administration of S1MP loaded with EphA2-siRNA-DOPC. Furthermore, a single administration of S1MP loaded with-EphA2-siRNA-DOPC substantially reduced tumor burden, angiogenesis, and cell proliferation compared with a noncoding control siRNA alone (SKOV3ip1, 54%; HeyA8, 57%), with no significant changes in serum chemistries or in proinflammatory cytokines. In summary, we have provided the first *in vivo* therapeutic validation of a novel, multistage siRNA delivery system for sustained gene silencing with broad applicability to pathologies beyond ovarian neoplasms.

Introduction

RNA interference (RNAi) therapy is emerging as a treatment modality of exceptional promise, in view of its versatile application to the silencing of any gene with a known sequence and especially those that are not drugable by existing approaches such as small-molecule inhibitors. However, *in vivo* systemic administration of RNAi has remained a major challenge due to its short half-life (1), lack of ability to penetrate the plasma membrane (2), and potential toxicity (3, 4). Nanoparticle-based delivery systems have been proposed to address these concerns. The validity of RNAi therapeutics has been shown in animal models (3, 5–7) and more recently in human clinical trials (8, 9). For all of the potential small interfering RNA (siRNA) delivery advantages they engender, nanoparticles also have some limitations including their potential for rapid clearance (10), instability in serum (11), and systemic toxicity, especially to the liver (3). Moreover, most of the current RNAi delivery approaches require frequent injections (12, 13), which can be a substantial impediment to patient treatment due to impaired enrollment on clinical trials and decreased patient compliance (14). Thus, development of safe, easy to administer, and efficient delivery systems that achieve sustained target gene silencing is of substantial clinical importance.

Previously, we have shown that siRNA incorporated in neutral nanoliposomes (30–40 nm in diameter) composed of dioleoyl phosphatidylcholine (DOPC) led to therapeutic gene modulation in several orthotopic cancer models with no overt toxicities (12, 13). Although our lipid-based siRNA delivery platform holds substantial promise for clinical translation, as is the case for other nanocarriers, our method currently requires twice weekly injections to achieve continuous gene silencing. We sought to develop a biocompatible approach that would allow for the sustained delivery of siRNA resulting in continuous gene silencing, therapeutic efficacy at nontoxic doses, and ease of administration. To attain these goals, we have developed a multistage delivery approach (Fig. 1A) composed of two biodegradable and biocompatible carriers: the first-stage carriers are mesoporous microscale biodegradable silicon particles (stage 1 micro-particles: S1MP; ref. 15), allowing for the loading and release of second-stage nanocarriers (DOPC nanoliposomal siRNA: siRNA-DOPC) in a sustained manner. Here, we provide the first evidence that a single administration of multistage siRNA-DOPC delivery resulted in sustained *in vivo* gene silencing for 3 weeks, significant antitumor effect in two orthotopic mouse models of human ovarian cancer with no observable concurrent toxicity.

Materials and Methods

Fabrication of porous silicon particles

Porous silicon particles were fabricated by electrochemical etching of silicon wafers as previously described (15). The physical dimension and pore size of S1MP were verified by

high-resolution scanning electron microscope. The porosity was verified by nitrogen absorption analysis as previously described (15).

Surface chemistry of S1MP

Surface of the S1MP was hydroxylated in oxygen plasma ($O_2$100sccm 50W). The positively charged amine groups were introduced on the surface by silanization with 9% v/v 3-aminopropyltriethoxysilane in isopropanol as previously described (15). The surface charge was measured by Zeta Pals (Brookhaven Instruments).

Liposomal siRNA formulation

The siRNA liposomes were prepared as previously described (13) by mixing 1,2 dioleoylsn-glycero-3-phosphocholine with siRNA (20:1, mol/mol) in the presence of excess *t*-butanol. Control siRNAs (5′-AATTCTCCGAACGTGTCACGT-3′) and Alexa 555–tagged control siRNA were purchased from Qiagen and siRNAs against EphA2 (5′-AATGACATGCCGATCTACATG-3′) were purchased from Sigma (16). Dry film of DOPC liposomes were reconstituted by adding water followed by briefly sonication.

Assembly of multistage vector

Amino functionalized S1MP (1×10^7 particles, 5 μg silicon) were mixed with *t*-butanol, and dried and mixed with DOPC nanoliposomes containing fluorescently labeled siRNA. The mixture was briefly sonicated and then spun down to remove any unincorporated free DOPC-siRNA. Fluorescence intensity of the supernatants as well as the precipitants were measured at Ex 555/Em 592 to assess loading efficacy.

Cell lines and culture

The human epithelial ovarian cancer cell lines such as HeyA8-Lc and Skov3ip1-Lc were used for these studies. Cells were maintained in RPMI 1640 supplemented with 15% fetal bovine serum and 0.1% gentamicin sulfate as described as previously (13). All experiments were performed with 70% to 80% confluent cultures.

Orthotopic *in vivo* model of ovarian cancer and tissue processing

Female athymic nude mice (NCr-nu; 4- to 5-weekold) were purchased from Taconic Farms and maintained as previously described (13). Institutional Animal Care and Use Committee approval was obtained before all animal studies. All mouse studies were approved by the M.D. Anderson Cancer Center Institutional Animal Care and Use Committee. Orthotopic nude mouse models of ovarian carcinoma (17) were used for this study as previously described.

Western blot analysis

Western blot was performed as previously described (13). Primary antibody against EphA2 was detected with horseradish peroxidase–conjugated IgG (Amersham) and developed using an enhanced chemiluminescence detection kit (Pierce). Membranes were tested for β-actin to confirm equal loading.

Immunohistochemistry

Ki67 and EphA2 staining were performed using formalin-fixed, paraffin-embedded tumor sections (8-μm thickness) as previously described (8). For the evaluation of cell proliferation, the proliferative indices were determined by counting the number of Ki67-positive cells out of total number of cells in five randomly selected high-power fields exclusive of necrotic areas at ×100 magnification. The data were expressed as percentage of

Ki67-positive cells. For the measurement of microvessel density, the proliferative indices were determined by counting the number of CD31-positive vessels in five randomly selected high-power fields exclusive of necrotic areas at ×100 magnification. All staining was quantified by two investigators in a blinded fashion.

Inductively coupled plasma atomic emission spectroscopy analysis for silicon content

The organs were lysed, spun down, and then analyzed for silicon content using inductively coupled plasma atomic emission spectroscopy. We detected silicon at 250.69, 251.43, 251.61, and 288.158 nm and Yttrium (1 ppm) was used as an internal control for normalization. All results were expressed as percent of injected dose.

Tissue transmission electron microscope (TEM)

The sections (100 nm) were imaged in a JEOL 1200 transmission electron microscope at 60 kV with digital images collected using a 1 k × 1 k Gatan BioScan camera Model 792.

Sample size justification and statistical analysis

We planed for $n = 10$ mice per treatment depending on the type of experiment. For an effect size (ratio of fixed effect and residual SD) of 0.65, this sample size was sufficient to provide 80% power for a test at significance level of 0.05. As part of preliminary analysis, we validated the normality assumption and proceeded with a nonparametric test as appropriate. The Mann-Whitney test was performed to compare the tumor sizes and tumor nodule number among different treatment groups.

In vivo safety study (blood chemistry and cytokine)

Plasma samples were collected from retro-orbital sinus and further analyzed for blood chemistry [lactate dehydrogenase (LDH), blood urea nitrogen (BUN), and creatinine] and proinflammatory cytokine production. Equivalent amounts of silicic acid (degradation product of silicon particles) and saline were used as negative controls. Cytokine levels in the supernatants were determined by ELISA kits according to the manufacturer's instructions (Bio-Rad).

Results

Assembly of multistage system loaded with neutral nanoliposomal siRNA (DOPC-siRNA)

We fabricated S1MP using electrochemical etching and photolithography as previously described (15). These methods allow for control over the size, shape, surface properties, overall porosity, and pore size of the S1MP. For this study, we used half-dome shaped S1MPs that were uniform in size with diameter of 1.6 ± 0.1 μm (Fig. 1A and C) and had straight pores in the center with average pore size of 26 nm (Fig. 1D). The size and shape for the S1MP were selected in accordance with the mathematical vector design criteria (18, 19). In particular, the S1MP design was chosen to enhance the probability of their margination and endothelial adhesion in capillary circulation. The S1MP were functionalized with an amine group to provide for a positive surface charge (8.0 mV) to enhance the charge-based interaction of negatively charged DOPC-siRNA (−2.9 mV) within the pores of the S1MP (Supplementary Fig. S1). We first examined the loading capacity of the S1MP to achieve the maximum loading of siRNA-DOPC. DOPC nanoliposomes containing Alexa555-labeled siRNA (Alexa555-siRNA-DOPC) were used for direct measurement of loading. Alexa555-siRNA-DOPC was efficiently incorporated into the S1MP in a concentration-dependent manner (Fig. 1E). Gel electrophoresis also supported siRNA-DOPC dose-dependent loading as well as the integrity of loaded siRNA (Fig. 1E). Under this loading condition, a maximum 2.0 pg of siRNA were loaded into a single S1MP (Fig. 1E). Effective loading of alexa555-

siRNA-DOPC was achievable when dried and positively charged S1MP was used (Supplementary Fig. S1), suggesting that the liposomes are loaded into the porous structure by capillary action. Approximately 35% of Alexa555-siRNA-DOPC were released from the S1MP within the first 3 hours (presumably associated with release from the surface and shallow pores), followed by gradual release of the remaining amount from the S1MP over 14 days (Fig. 1F).

Effect of multistage delivery on siRNA tumor uptake and tissue distribution

To determine the duration and extent of siRNA-DOPC delivery *in vivo*, we first compared siRNA distribution and tumor uptake using the S1MP loaded with Alexas555-siRNA-DOPC versus Alexas555-siRNA-DOPC alone. Mice with HeyA8 orthotopic tumors (15 days after i.p. inoculation of tumor cells) were given an i.v. injection of either S1MP loaded with a single dose of Alexa555-siRNA-DOPC (5 μg siRNA) or a single dose of Alexa555-siRNA-DOPC alone (5 μg siRNA). At day 10, siRNA fluorescence was almost absent in the tumors from mice treated with Alexa555-siRNA-DOPC, whereas fluorescence remained for >10 days in the tumor from mice injected with S1MP-Alexa555-siRNA-DOPC (Supplementary Fig. S2A). Overall, a single injection of the S1MP loaded with siRNA-DOPC resulted in enhanced siRNA uptake into the tumor parenchyma by 6-fold compared with siRNA-DOPC alone. No significant difference in Alexa555-siRNA uptake into other organs such as kidney or liver was noted (Supplementary Fig. S2B and C).

In vivo delivery of siRNA-DOPC using the multistage system

Based on the sustained delivery observed in the experiments noted above, we next investigated the duration and extent of gene silencing. We focused on EphA2 (receptor tyrosine kinase in the ephrin family; ref. 20) because EphA2 is overexpressed in >70% of ovarian cancers and is associated with poor patient outcome (21). We first evaluated the immunostimulatory potential of EphA2 siRNA and/or the DOPC nanoliposomes because immunologic effects, especially with certain sequences and delivery vehicles, have been reported (22, 23). There were no biologically meaningful alterations noted in the cytokines tested (Supplementary Fig. S3; ref. 24). We then optimized the siRNA dose required for sustained gene silencing. Mice bearing SKOV3ip1 ovarian tumors were given an i.v. injection of S1MP loaded with either single-dose EphA2-siRNA-DOPC (5 μg EphA2-siRNA) or triple-dose EphA2-siRNA-DOPC (15 μg EphA2-siRNA). The mice were sacrificed (three mice per time point) and the tumors were harvested at indicated time points and assessed for EphA2 protein expression level (Fig. 2). A single administration of triple-dose S1MP-EphA2-siRNA-DOPC resulted in >80% reduction of EphA2 expression and this effect lasted for 3 weeks (Fig. 2A and B), whereas typically a single injection of EphA2-siRNA-DOPC alone silenced EphA2 expression for only up to 5 to 6 days (13). S1MP loaded with a single dose of EphA2-siRNA-DOPC failed to silence EphA2 gene expression (data not shown). Sustained gene silencing in the tumor was also supported by immunohistochemical analysis, which showed EphA2 downregulation for 28 days (Fig. 2C). This sustained *in vivo* gene silencing in the tumor for at least 3 to 4 weeks following a single injection is a major technical advance over frequent repetitive dosing.

Therapeutic effect of the multistage delivery of EphA2-siRNA-DOPC

Because multistage delivery of siRNA-DOPC resulted in sustained gene silencing, we next tested the antitumor activity of this delivery method. Mice were treated either twice weekly with siRNA-DOPC (5 μg EphA2-siRNA per injection, for a total administered dose of 30 μg EphA2-siRNA over 3 weeks) or a single administration with S1MP-EphA2-siRNA-DOPC (15 μg EphA2-siRNA). No abnormal behavior or weight loss was noted during the entire treatment period (Supplementary Fig. S4). Treatment with S1MP-EphA2-siRNA-DOPC in mice with SKOV3ip1 tumor significantly reduced tumor weight by 54.2% and

65.3% compared with nonsilencing control siRNA-DOPC and S1MP- nonsilencing control-siRNA-DOPC, respectively ($P < 0.05$; ANOVA F = 4.92). Similarly, significant tumor weight reduction was observed in the HeyA8 model treated with S1MP-EphA2-siRNA-DOPC compared with nonsilencing control DOPC (57.4%) and S1MP-nonsilencing control-siRNA-DOPC (69.3%), respectively ($P < 0.01$; ANOVA F = 5.89; Fig. 3A and B). These data show that a single administration of S1MP-EphA2-siRNA-DOPC led to a comparable antitumor effect to six repeated i.v. injections of EphA2-siRNA-DOPC for a total of twice the siRNA dosage administered by the multistage strategy. The number of nodules formed was also comparably reduced by both S1MP-EphA2-siRNA-DOPC and EphA2-siRNA-DOPC in the SKOV3ip1 model (Supplementary Fig. S5). Tumor-bearing mice treated with either S1MP-EphA2-siRNA-DOPC or EphA2-siRNA-DOPC alone did not develop ascites, in contrast with control mice treated with either saline, S1MP alone, nonsilencing-siRNA-DOPC, or S1MP-nonsilencing-siRNA-DOPC (Supplementary Fig. S6). We assessed the biological effect of sustained downregulation of EphA2 by determining microvessel density (CD31) and cell proliferation (Ki67). Representative sections from each treatment group are shown with mean number of vessels per field or mean percent of proliferative cells. Compared with control groups, the mean microvessel density was significantly reduced by ~3-fold in tumors treated with both S1MP-EphA2-siRNA-DOPC and EphA2-siRNA-DOPC (overall ANOVA: **, $P < 0.001$; Fig. 4). Similarly, proliferation index was also significantly reduced by 20-fold when mice were treated with both S1MP-EphA2- siRNA-DOPC and EphA2-siRNA-DOPC (overall ANOVA: **, $P < 0.001$; Fig. 4).

Biodistribution and biodegradation of S1MP

To examine the biodistribution of S1MP, the mice were injected with Alexa555-siRNA-DOPC loaded S1MP i.v. and the major organs including liver, kidney, spleen, lung, and heart were harvested 4 hours after the injection. Silicon content analysis showed that S1MP were primarily accumulated in the liver (53%) and spleen (11% of total injected dose), and there was no to minimal S1MP accumulation observed in the kidney, lung, and heart (Fig. 5A). To provide further evidence that the S1MP allows sustained siRNA release, S1MP conjugated with FITC (green fluorescence) were loaded with Alexa555-siRNA-DOPC (red fluorescence) and i.v. injected into mice. The liver and spleen were harvested 20 days after injection for histologic evaluation. Alexa555-siRNA-DOPC remained associated with S1MP as evidenced by the yield of yellow fluorescence, but not with macrophages (pink) in the liver and spleen at 20 days after injection (Supplementary Fig. S7A and B), indicating that Alexa555-siRNA-DOPC remains intact. The S1MP were distributed throughout the liver sinusoids and the red pulp in the spleen (Fig. 5B). Histopathologic analyses of tissue sections with H&E stain showed no obvious inflammatory infiltration in these organs. In the liver, the S1MPs were distributed throughout the sinusoids and (Fig. 5B) some were taken up by Kupffer cells (Supplementary Fig. S7A). In the spleen, the S1MPs were present in the splenic cords (Fig. 5B) and some were taken up by f4/80-positive macrophages (Supplementary Fig. S7B). Transmission electron microscopic analyses of the liver and spleen sections confirmed that S1MP remained within sinusoidal spaces in the liver and red pulp in the spleen (Fig. 5C). Silicon contents in the spleen were reduced by 80% in the first 2 weeks and cleared by the 3rd week (Fig. 6A). In contrast, only 55% of S1MP was cleared from the liver in the first 2 weeks and ~25% of the injected S1MP remained in the liver 3 weeks after injection (Fig. 6B), suggesting that S1MP degradation kinetics are different in each organ. Scanning electron microscopic images of S1MP showed enlargement of pore size at day 7 and reduction of overall size by day 14 (Fig. 6C). In some cases, bulky surface erosion was noted (data not shown). Collectively, these data suggest that the S1MP serve as a reservoir to protect siRNA-DOPC from degradation, release them over time by a mechanism that combines degradation of the carrier material, and hindered diffusion through the nanoscopic pore.

Biocompatibility of S1MP

We next tested the biocompatibility of multistage delivery system in both an acute and chronic setting in FBV/N mice following the i.v. administration of therapeutic dose of S1MP-EphA2-siRNA-DOPC (15 μg EphA2-siRNA). Blood chemistry showed that S1MPs did not cause a significant increase in any of the parameters tested (Supplementary Fig. S8A–F). Despite significant accumulation of the S1MP in the liver and spleen, plasma LDH levels from the liver and spleen remained unchanged (Supplementary Fig. S8A and D). Similarly, tissue LDH levels in the liver and spleen were not changed at both conditions tested (data not shown), indicating that accumulation of the S1MP in the liver and spleen did not cause tissue injury. Similar to blood chemistry, the values of cytokines tested were not significantly higher in the mice injected with DOPC-loaded S1MP than in the saline-injected control animals in both acute and chronic setting, although some S1MP were taken up by macrophages (Supplementary Fig. S8G and H). These data indicate that S1MP-siRNA-DOPC is not toxic to the kidney, liver, and spleen and that no significant levels of inflammatory cytokines were induced by the S1MP or its degradation products.

Discussion

The key findings from this work are that a single injection of multistage delivery system comprised mesoporous silicon particles loaded with liposomal siRNA against oncogene, EphA2, resulted in a sustained gene silencing for up to at least 3 weeks in ovarian tumor, concomitant with a substantial reduction of tumor burden with no to minimum toxicity. Many oncoproteins as well as their distinct roles have been identified in the past few decades; however, many of them are “undrugable” with traditional approaches such as small-molecule inhibitors because their crystal structures are unknown. We targeted oncoprotein EphA2 (tyrosine kinase receptor in the ephrin family), which plays roles in angiogenesis (25) and cell proliferation (26), and is difficult to target with conventional approaches. EphA2 is absent in the normal tissue but is overexpressed in different types of tumor including ovarian (27), breast (28), lung (29), and melanoma (30), with strong association with poor survival, advanced-stage, or high-metastatic potential (31). Although the dual roles of EphA2 as a pro-oncogenic or antioncogenic protein have been suggested (32), a recent study revealed that EphA2 mediates cell migration and invasion in the absence of ephrin (a cognate ligand for EphA2) through Akt phosphorylation (33). It has also been reported that EphA2 overexpression is frequently accompanied by the loss of ephrin, further supporting the pro-oncogenic role of EphA2 in cancer (34). Therefore, a disruption of the biological functions of EphA2 is a highly attractive molecular-targeted therapy approach (35).

Our data shown that the multistage delivery of liposomal siRNA (single injection of 15 μg EphA2-siRNA) led to comparable antitumor effect to repeated i.v. siRNA-DOPC injections (six injections of 5 μg EphA2-siRNA each), thus halving the siRNA dosage required to achieve an equivalent antitumor effect. Although we are focusing on EphA2 in this study, this platform could allow for highly adjustable personalized molecular targeted therapies with a suitable combination of RNAi depending on the molecular signature of each tumor type with “tunable” release kinetics of siRNA to control cancer cell growth. Many efforts have been reported to deliver RNAi; viral vectors (36), chemically modified siRNA (6), and nonviral nanocarriers including cationic liposome (37) and polycation-based carriers (38) have shown effective gene silencing effects *in vitro* and *in vivo*. However, immunogenicity, toxicity, safety concern, and unfavorable pharmacokinetics remain generally unsolved problems for these delivery strategies. Traditional approaches to the improvement of pharmacokinetics include surface functionalization of nanocarrier with polyethylene glycol (PEG) to avoid reticuloendothelial system uptake (39). PEG, however, does not prevent renal excretion and degradation of nanocarriers. In addition, PEGylation accelerates the

clearance of nanocarrier from the circulation when injected repeatedly (40). Thus, with the aim of providing stability to nanocarriers containing biologically active payload and of achieving sustainedgene silencing, in this study, we used mesoporous silicon particles (S1MP) as a carrier of DOPC neutral nanoliposomes. The serum half-life ($t_{1/2}$) of systemically injected DOPC nanoliposomes is ~2.7 hours.12 The combinatorial multistage delivery system we used in this study significantly improved the pharmacokinetics of the DOPC liposome and resulted in 3-week-long sustained gene silencing of EphA2 in the tumor. It is likely that S1MP protect DOPC- siRNA from degradation and renal excretion due to their entrapment within the capillary spaces within the liver and spleen (Fig. 5). Slow release is most likely attained due to the gradual degradation of S1MP with subsequent release of siRNA-DOPC that reaches to the tumor.

Porous silicon is an attractive material (41), which has been investigated for possible applications in drug delivery by loading of nanoscale payload such as protein (42), enzymes (43), drugs (41), and nanocarriers (15). The surface chemistry on the porous silicon will play a critical role in determining the loading efficacy and release kinetics based on the type of interaction of payload and porous surface (41). We used positively charged S1MP for enhanced entrapment of the negatively charged (−2.9 mV) DOPC-siRNA. The electrostatic interactions between the pore wall surface and liposomes are likely to contribute to the sustained release of the liposomes from the porous structure as the S1MP degrades.

Mesoporous silicon is biocompatible (44, 45) and has received Food and Drug Administration approval for use in brachytherapy and drug delivery from implants (BioSilicon; ref. 46). The two delivery carrier materials used in this study, mesoporous silicon and DOPC neutral liposome, are highly biodegradable, biocompatible, and combine suitably to yield time-sustained delivery with no liver and renal toxicity in both in the acute and the chronic setting, at a dose of 25 μg of mesoporous silicon (Supplementary Fig. S8). In a separate study, we showed the safe systemic administration of 250 μg of mesoporous (10-fold the dose used here) through both i.p. and i.v. routes in mice.13 The multistage delivery system used in this study did not result in the production of the proinflammatory cytokines tested, unlike other delivery system that relies on the host immunity (47). Our data indicate that the antitumor effect mediated by the S1MP loaded with DOPC-siRNA was due to the DOPC-siRNA-EphA2 mediated gene silencing of EphA2 and not due to immunostimulatory effects.

Porous silicon is known to degrade completely into orthosilicic acid over time, which is readily excreted from the body. The mechanism of sustained liposomal siRNA delivery is likely to rely on essentially two unique characteristics and tailorable characteristics of the S1MP: biodegradation and biodistribution. Biodegradation is controlled by the overall porosity and pore size of the particles (48), which in turn is exquisitely controllable by choice of material processing parameters (41). The biodistribution of the particles is controlled by their size, shape, surface, and bulk properties (49), which are also precisely controlled during the particle fabrication processes (15). In view of the different degradation kinetics in different organs, and in particular within the liver and the spleen, altering their respective accumulations will lead to different, adjustable kinetics of release of the nanoliposome-encapsulated siRNA. Possible mechanisms involved in the geometry-dependent organ sequestration of particles are capillary size, capillary architecture, hemodynamics, and endocytosis (49).

[12]R.A. Nieves, T. Tanaka, C. Rodriguez-Aguayo, T. Madden, A.M. Tari, A.K. Sood, M. Ferrari, G. Lopez-Berestein, unpublished data.

[13]T. Tanaka, B. Godin, R. Bhavane, R.A. Nieves, J. Gu, X. Liu, C. Chiappini, J.R. Fakhoury, S. Amra, A. Ewing, Q. Li, M. Ferrari, unpublished data.

In conclusion, in this study, we showed that a single injection of multistage delivery system comprised of mesoporous silicon particles loaded with nanoliposomal siRNA against oncogene, EphA2, resulted in: (*a*) sustained gene silencing for up to at least 3 weeks in ovarian tumor; (*b*) substantial reduction of tumor burden; (*c*) substantial decrease of angiogenesis and cellular proliferation; (*d*) no production of ascites; and (*e*) no detected toxicity associated with the S1MP vectors, the neutral nanoliposomes, or the therapeutic siRNA. To the best of our knowledge, this is the first study to achieve these collective goals *in vivo* and, in particular, in two orthotopic models of ovarian cancer. These finding encourage the development of a “library” of targets and drugs that can be further tailored toward specific genetic abnormalities in cancer.

Supplementary Material

Refer to Web version on PubMed Central for supplementary material.

Acknowledgments

We thank Matthew Landry for assistance with manuscript preparation.

Grant Support

Department of Defense (W81XWH-07-2-0101, W81XWH-09-1-0212) and NIH (R01CA128797, R33CA122864), the State of Texas's Emerging Technology Fund, National Aeronautics and Space Administration (NNJ06HE06A), the Ovarian Cancer Research Fund Program Project Development Grant, the University of Texas M.D. Anderson Cancer Center Ovarian Cancer Specialized Program of Research Excellence (P50 CA083639), the NIH (CA110793, CA109298), the Zarrow Foundation, the Betty Ann Asche Murray Distinguished Professorship, the Baylor WRHR grant (HD050128) and the GCF Molly-Cade ovarian cancer research grant (M.M.K. Shahzad), and the Alliance for NanoHealth.

References

1. Bumcrot D, Manoharan M, Koteliansky V, Sah DW. RNAi therapeutics: a potential new class of pharmaceutical drugs. Nat Chem Biol. 2006; 2:711–719. [PubMed: 17108989]
2. Aagaard L, Rossi JJ. RNAi therapeutics: principles, prospects and challenges. Adv Drug Deliv Rev. 2007; 59:75–86. [PubMed: 17449137]
3. Heidel JD, Yu Z, Liu JY, et al. Administration in non-human primates of escalating intravenous doses of targeted nanoparticles containing ribonucleotide reductase subunit M2 siRNA. Proc Natl Acad Sci U S A. 2007; 104:5715–5721. [PubMed: 17379663]
4. Desai AA, Schilsky RL, Young A, et al. A phase I study of antisense oligonucleotide GTI-2040 given by continuous intravenous infusion in patients with advanced solid tumors. Ann Oncol. 2005; 16:958–965. [PubMed: 15824081]
5. Frank-Kamenetsky M, Grefhorst A, Anderson NN, et al. Therapeutic RNAi targeting PCSK9 acutely lowers plasma cholesterol in rodents and LDL cholesterol in nonhuman primates. Proc Natl Acad Sci U S A. 2008; 105:11915–11920. [PubMed: 18695239]
6. Morrissey DV, Lockridge JA, Shaw L, et al. Potent and persistent *in vivo* anti-HBV activity of chemically modified siRNAs. Nat Biotechnol. 2005; 23:1002–1007. [PubMed: 16041363]
7. Zimmermann TS, Lee AC, Akinc A, et al. RNAi-mediated gene silencing in non-human primates. Nature. 2006; 441:111–114. [PubMed: 16565705]
8. Kim DH, Rossi JJ. Strategies for silencing human disease using RNA interference. Nat Rev Genet. 2007; 8:173–184. [PubMed: 17304245]
9. Davis ME. The first targeted delivery of siRNA in humans via a self-assembling, cyclodextrin polymer-based nanoparticle: from concept to clinic. Mol Pharm. 2009; 6:659–668. [PubMed: 19267452]
10. Longmire M, Choyke PL, Kobayashi H. Clearance properties of nano-sized particles and molecules as imaging agents: considerations and caveats. Nanomedicine. 2008; 3:703–717. [PubMed: 18817471]

11. Zhang Y, Bradshaw-Pierce EL, Delille A, Gustafson DL, Anchordoquy TJ. *In vivo* comparative study of lipid/DNA complexes with different *in vitro* serum stability: effects on bio-distribution and tumor accumulation. J Pharm Sci. 2008; 97:237–250. [PubMed: 17721944]
12. Merritt WM, Lin YG, Spannuth WA, et al. Effect of interleukin-8 gene silencing with liposome-encapsulated small interfering RNA on ovarian cancer cell growth. J Natl Cancer Inst. 2008; 100:359–372. [PubMed: 18314475]
13. Landen CN Jr, Chavez-Reyes A, Bucana C, et al. Therapeutic EphA2 gene targeting *in vivo* using neutral liposomal small interfering RNA delivery. Cancer Res. 2005; 65:6910–6918. [PubMed: 16061675]
14. Lara PN Jr, Higdon R, Lim N, et al. Prospective evaluation of cancer clinical trial accrual patterns: identifying potential barriers to enrollment. J Clin Oncol. 2001; 19:1728–1733. [PubMed: 11251003]
15. Tasciotti E, Liu XW, Bhavane R, et al. Mesoporous silicon particles as a multistage delivery system for imaging and therapeutic applications. Nat Nanotechnol. 2008; 3:151–157. [PubMed: 18654487]
16. Halder J, Kamat AA, Landen CN Jr, et al. Focal adhesion kinase targeting using *in vivo* short interfering RNA delivery in neutral liposomes for ovarian carcinoma therapy. Clin Cancer Res. 2006; 12:4916–4924. [PubMed: 16914580]
17. Thaker PH, Yazici S, Nilsson MB, et al. Antivascular therapy for orthotopic human ovarian carcinoma through blockade of the vascular endothelial growth factor and epidermal growth factor receptors. Clin Cancer Res. 2005; 11:4923–4933. [PubMed: 16000591]
18. Decuzzi P, Ferrari M. The adhesive strength of non-spherical particles mediated by specific interactions. Biomaterials. 2006; 27:5307–5314. [PubMed: 16797691]
19. Decuzzi P, Lee S, Decuzzi M, Ferrari M. Adhesion of microfabricated particles on vascular endothelium: a parametric analysis. Ann Biomed Eng. 2004; 32:793–802. [PubMed: 15255210]
20. Stein E, Lane AA, Cerretti DP, et al. Eph receptors discriminate specific ligand oligomers to determine alternative signaling complexes, attachment, and assembly responses. Gene Dev. 1998; 12:667–678. [PubMed: 9499402]
21. Lin YG, Han LY, Kamat AA, et al. EphA2 overexpression is associated with angiogenesis in ovarian cancer. Cancer. 2007; 109:332–340. [PubMed: 17154180]
22. Judge AD, Sood V, Shaw JR, Fang D, McClintock K, MacLachlan I. Sequence-dependent stimulation of the mammalian innate immune response by synthetic siRNA. Nat Biotechnol. 2005; 23:457–462. [PubMed: 15778705]
23. Robbins MA, Rossi JJ. Sensing the danger in RNA. Nat Med. 2005; 11:250–251. [PubMed: 15746933]
24. Mangala LS, Zuzel V, Schmandt R, et al. Therapeutic targeting of ATP7B in ovarian carcinoma. Clin Cancer Res. 2009; 15:3770–3780. [PubMed: 19470734]
25. Ogawa K, Pasqualini R, Lindberg RA, Kain R, Freeman AL, Pasquale EB. The ephrin-A1 ligand and its receptor, EphA2, are expressed during tumor neovascularization. Oncogene. 2000; 19:6043–6052. [PubMed: 11146556]
26. Cheng N, Brantley DM, Liu H, et al. Blockade of EphA receptor tyrosine kinase activation inhibits vascular endothelial cell growth factor-induced angiogenesis. Mol Cancer Res. 2002; 1:2–11. [PubMed: 12496364]
27. Thaker PH, Deavers M, Celestino J, et al. EphA2 expression is associated with aggressive features in ovarian carcinoma. Clin Cancer Res. 2004; 10:5145–5150. [PubMed: 15297418]
28. Zelinski DP, Zantek ND, Stewart JC, Irizarry AR, Kinch MS. EphA2 overexpression causes tumorigenesis of mammary epithelial cells. Cancer Res. 2001; 61:2301–2306. [PubMed: 11280802]
29. Kinch MS, Moore MB, Harpole DH Jr. Predictive value of the EphA2 receptor tyrosine kinase in lung cancer recurrence and survival. Clin Cancer Res. 2003; 9:613–618. [PubMed: 12576426]
30. Easty DJ, Hill SP, Hsu MY, et al. Up-regulation of ephrin-A1 during melanoma progression. Int J Cancer. 1999; 84:494–501. [PubMed: 10502726]

31. Kertesz N, Krasnoperov V, Reddy R, et al. The soluble extracellular domain of EphB4 (sEphB4) antagonizes EphB4-2 interaction, modulates angiogenesis, and inhibits tumor growth. Blood. 2006; 107:2330–2338. [PubMed: 16322467]
32. Miao H, Wei BR, Peehl DM, et al. Activation of EphA receptor tyrosine kinase inhibits the Ras/MAPK pathway. Nat Cell Biol. 2001; 3:527–530. [PubMed: 11331884]
33. Miao H, Li DQ, Mukherjee A, et al. EphA2 mediates ligand-dependent inhibition and ligand-independent promotion of cell migration and invasion via a reciprocal regulatory loop with Akt. Cancer Cell. 2009; 16:9–20. [PubMed: 19573808]
34. Dodelet VC, Pasquale EB. Eph receptors and ephrin ligands: embryogenesis to tumorigenesis. Oncogene. 2000; 19:5614–5619. [PubMed: 11114742]
35. Lee JW, Han HD, Shahzad MM, et al. EphA2 immunoconjugate as molecularly targeted chemotherapy for ovarian carcinoma. J Natl Cancer Inst. 2009; 101:1193–1205. [PubMed: 19641174]
36. Xia H, Mao Q, Paulson HL, Davidson BL. siRNA-mediated gene silencing *in vitro* and *in vivo*. Nat Biotechnol. 2002; 20:1006–1010. [PubMed: 12244328]
37. Schiffelers RM, Ansari A, Xu J, et al. Cancer siRNA therapy by tumor selective delivery with ligand-targeted sterically stabilized nanoparticle. Nucleic Acids Res. 2004; 32:e149. [PubMed: 15520458]
38. Bitko V, Musiyenko A, Shulyayeva O, Barik S. Inhibition of respiratory viruses by nasally administered siRNA. Nat Med. 2005; 11:50–55. [PubMed: 15619632]
39. Wang S, Lee RJ, Cauchon G, Gorenstein DG, Low PS. Delivery of antisense oligodeoxyribonucleotides against the human epidermal growth factor receptor into cultured KB cells with liposomes conjugated to folate via polyethylene glycol. Proc Natl Acad Sci U S A. 1995; 92:3318–3322. [PubMed: 7724560]
40. Laverman P, Carstens MG, Boerman OC, et al. Factors affecting the accelerated blood clearance of polyethylene glycolliposomes upon repeated injection. J Pharmacol Exp Ther. 2001; 298:607–612. [PubMed: 11454922]
41. Anglin EJ, Cheng L, Freeman WR, Sailor MJ. Porous silicon in drug delivery devices and materials. Adv Drug Deliv Rev. 2008; 60:1266–1277. [PubMed: 18508154]
42. Foraker AB, Walczak RJ, Cohen MH, Boiarski TA, Grove CF, Swaan PW. Microfabricated porous silicon particles enhance paracellular delivery of insulin across intestinal Caco-2 cell monolayers. Pharm Res. 2003; 20:110–116. [PubMed: 12608544]
43. Delouise LA, Miller BL. Enzyme immobilization in porous silicon: quantitative analysis of the kinetic parameters for glutathione-S-transferases. Anal Chem. 2005; 77:1950–1956. [PubMed: 15801723]
44. Prestidge CA, Barnes TJ, Lau CH, Barnett C, Loni A, Canham L. Mesoporous silicon: a platform for the delivery of therapeutics. Expert Opin Drug deliv. 2007; 4:101–110. [PubMed: 17335408]
45. Park JH, Gu L, von Maltzahn G, Ruoslahti E, Bhatia SN, Sailor MJ. Biodegradable luminescent porous silicon nanoparticles for *in vivo* applications. Nat Mater. 2009; 8:331–336. [PubMed: 19234444]
46. Zhang K, Loong SL, Connor S, et al. Complete tumor response following intratumoral 32P BioSilicon on human hepatocellular and pancreatic carcinoma xenografts in nude mice. Clin Cancer Res. 2005; 11:7532–7537. [PubMed: 16243828]
47. Cubillos-Ruiz JR, Engle X, Scarlett UK, et al. Polyethylenimine-based siRNA nanocomplexes reprogram tumor-associated dendritic cells via TLR5 to elicit therapeutic antitumor immunity. J Clin Invest. 2009; 119:2231–2244. [PubMed: 19620771]
48. Canham LT. Bioactive silicon structure fabrication through nanoetching techniques. Adv Mater. 1995; 7:1033–1037.
49. Decuzzi P, Pasqualini R, Arap W, Ferrari M. Intravascular delivery of particulate systems: Does geometry really matter? Pharm Res. 2009; 26:235–243. [PubMed: 18712584]

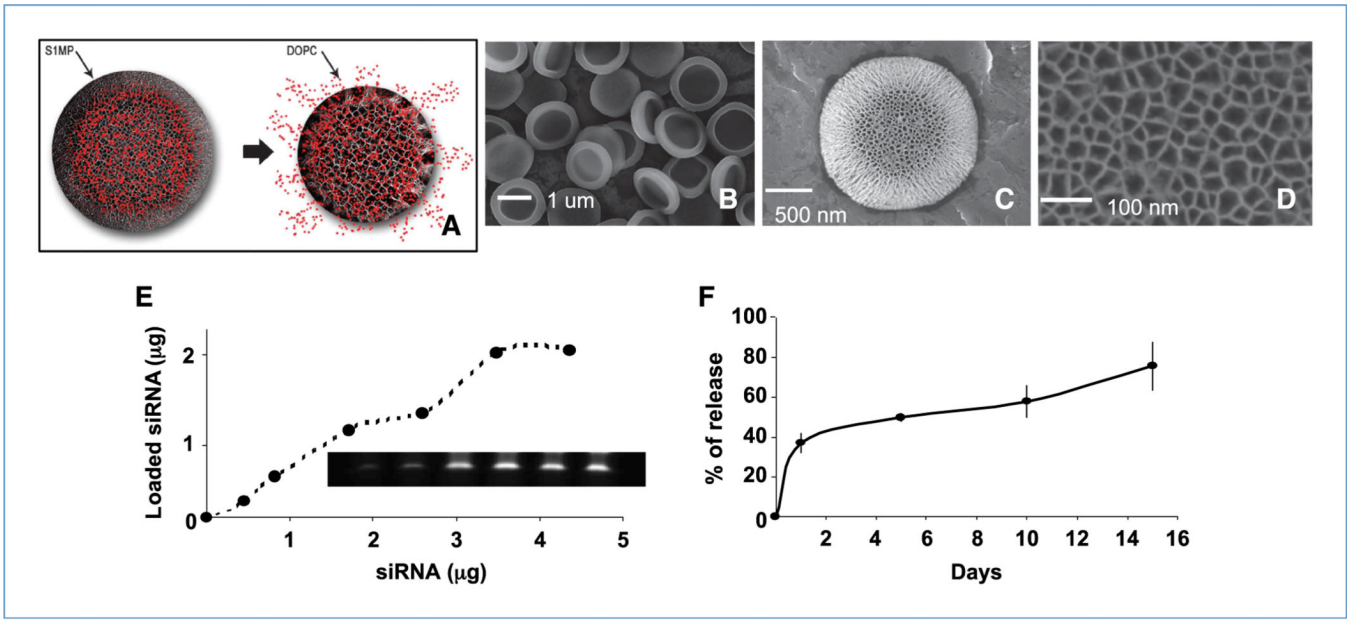

Figure 1.

Assembly of S1MP-siRNA-DOPC. A, concept of multistage delivery system. B to D, Scanning electron microscopic images of S1MP at different magnifications. E, loading of Alexa555-siRNA-DOPC to the S1MP. After the loading, fluorescence from unincorporated Alexa555-siRNA-DOPC was measured to assess the loading efficacy. S1MP loaded with Alexa555-siRNA-DOPC were dissolved in 0.25% tetramethylammonium hydroxide and the loaded siRNA were separated by gel electrophoresis and visualized with SYBR Gold. F, release kinetics of Alexa555-siRNA-DOPC from the S1MP. The Alexa555-siRNA-DOPC–loaded S1MP were incubated in 10% FBS and the supernatant was separated to measure fluorescent intensity at Ex544/Em590 at different time points.

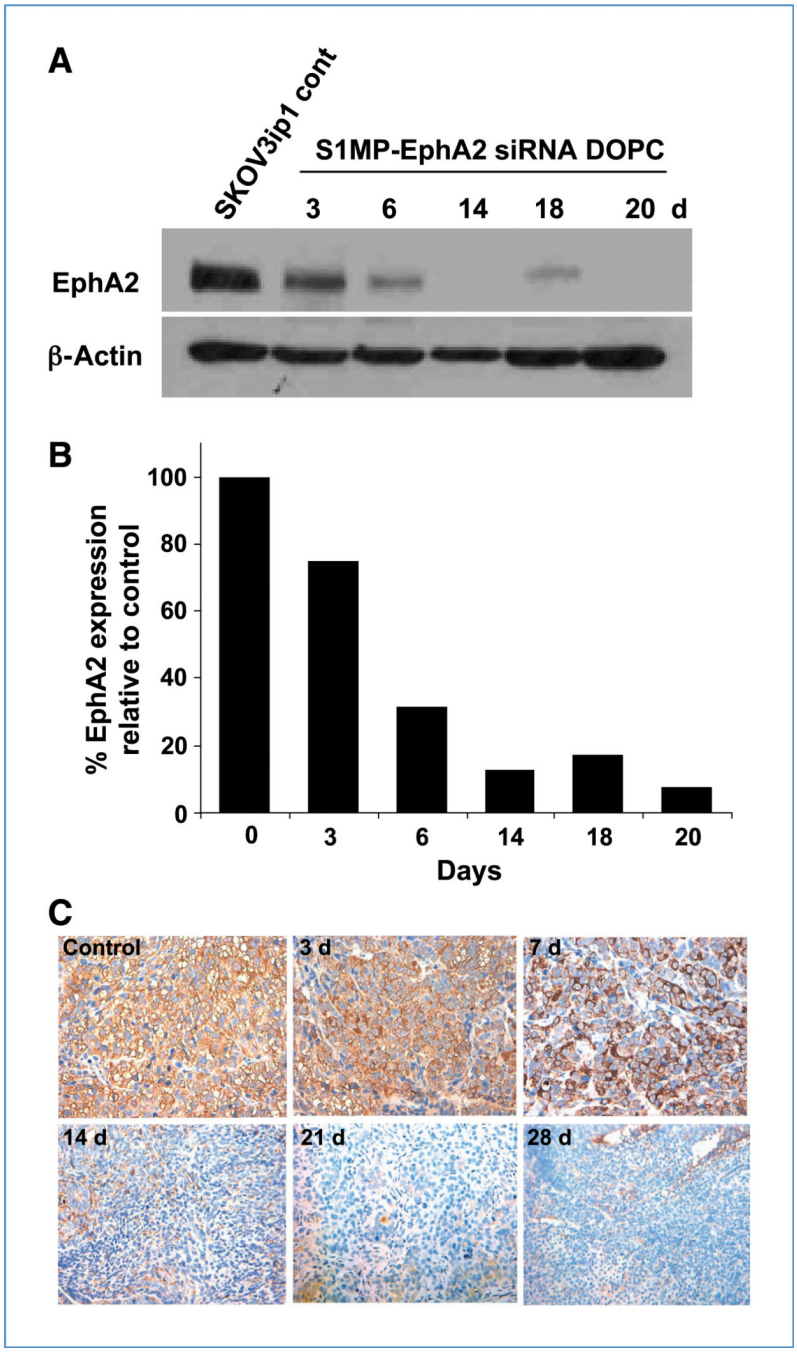

Figure 2.

Systemic delivery of siRNA-DOPC using S1MP results in long-lasting *in vivo* gene silencing. The mice (three mice per time point) bearing SKOV3ip1 orthotopic ovarian tumors were injected with S1MP-EphA2-siRNA-DOPC or left nontreated. A, the tumors were harvested at the indicated time points for Western blot to measure EphA2 expression levels. Thirty micrograms of tumor lysate were separated on a 10% SDS-PAGE and transferred on to a polyvinylidene difluoride membrane. The membrane was incubated with anti-EphA2 antibody overnight at 4°C. The membrane was tested for β-actin to confirm equal loading. B, densitometric analysis was performed to normalize EphA2 expression by β-actin. Data were expressed as % of normalized value to the nontreated. C,

immunohistochemical analysis of EphA2 expression in the SKOV1ip3 tumor. Images were taken at original magnification of ×400.

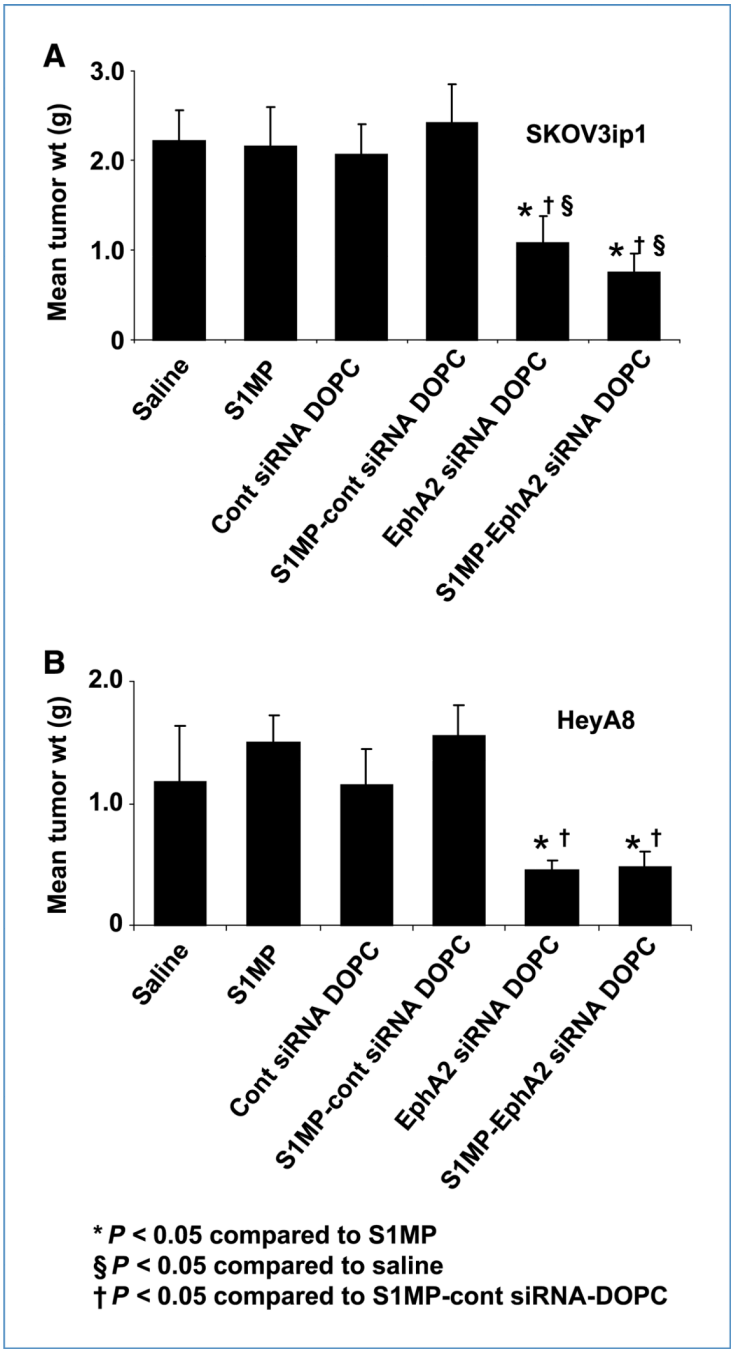

Figure 3.

Therapeutic efficacy of sustained EphA2-siRNA-DOPC delivery by S1MP. Nude mice were injected i.p. with SKOV3ip1 or HeyA8 cells and randomly allocated to one of six treatment groups ($n = 10$): (*a*) saline, (*b*) S1MP, (*c*) nonsilencing control siRNA-DOPC, (*d*) S1MP-nonsilencing control-siRNA-DOPC, (*e*) EphA2-siRNA-DOPC, (*f*) S1MP-EphA2-siRNA-DOPC. SiRNA-DOPC was i.v. injected biweekly at a dose of 5 μg siRNA. S1MP-EphA2-siRNA-DOPC was injected in a single administration in 3 wks at a dose of 15 μg siRNA. The mice were injected with saline biweekly in the rest of treatment period. When control animals (saline- and nonsilencing siRNA–treated mice) began to appear moribund (4–5 wks after cell injection), all animals in an experiment were sacrificed and mouse weight, tumor

weight (wt), tumor number, ascites volume, and tumor location were recorded. Columns, mean tumor weight from SKOV3ip1 (A) or HeyA8 cells (B); bars, SD.

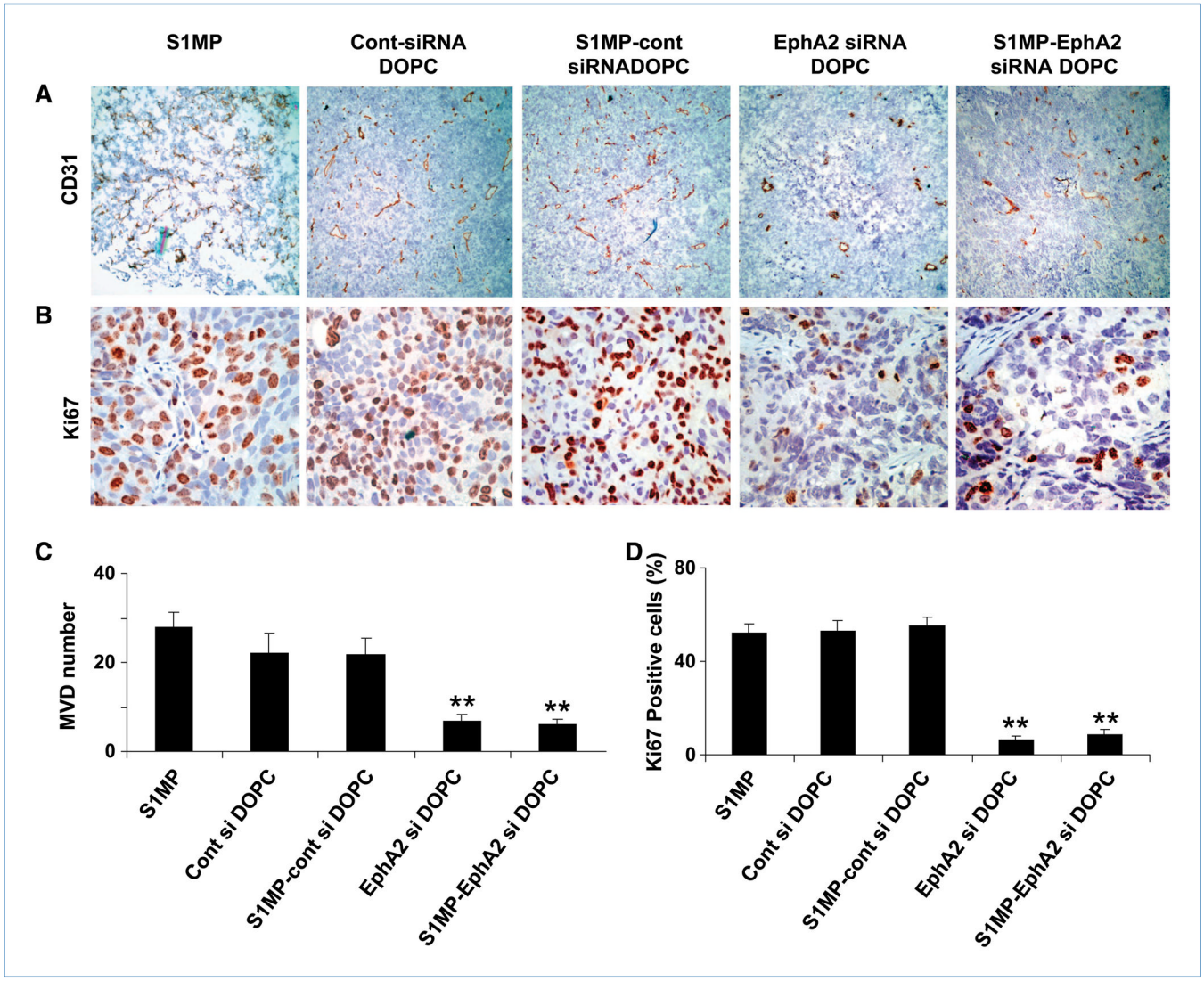

Figure 4.

Effect of sustained siRNA delivery on angiogenesis and cell proliferation. Tumors from animals with the SKOV3ip1 ovarian tumor were examined for microvessel density (CD31) and cell proliferation (Ki67). Representative sections from each treatment group are shown (final magnification, ×100 for CD31 and ×400 for Ki67), with mean number of vessels per field or mean % of proliferative cells, summarized in the graph at the bottom. Five different fields per slides, at least three individual tumors per treatment group were examined. Both microvessel density (MVD; A and C) and cell proliferation (B and D) were significantly reduced in tumor when treated with repeated administration of EphA2-siRNA-DOPC and a single administration of the S1MP-EphA2-siRNA-DOPC. (overall ANOVA: **, $P < 0.001$).

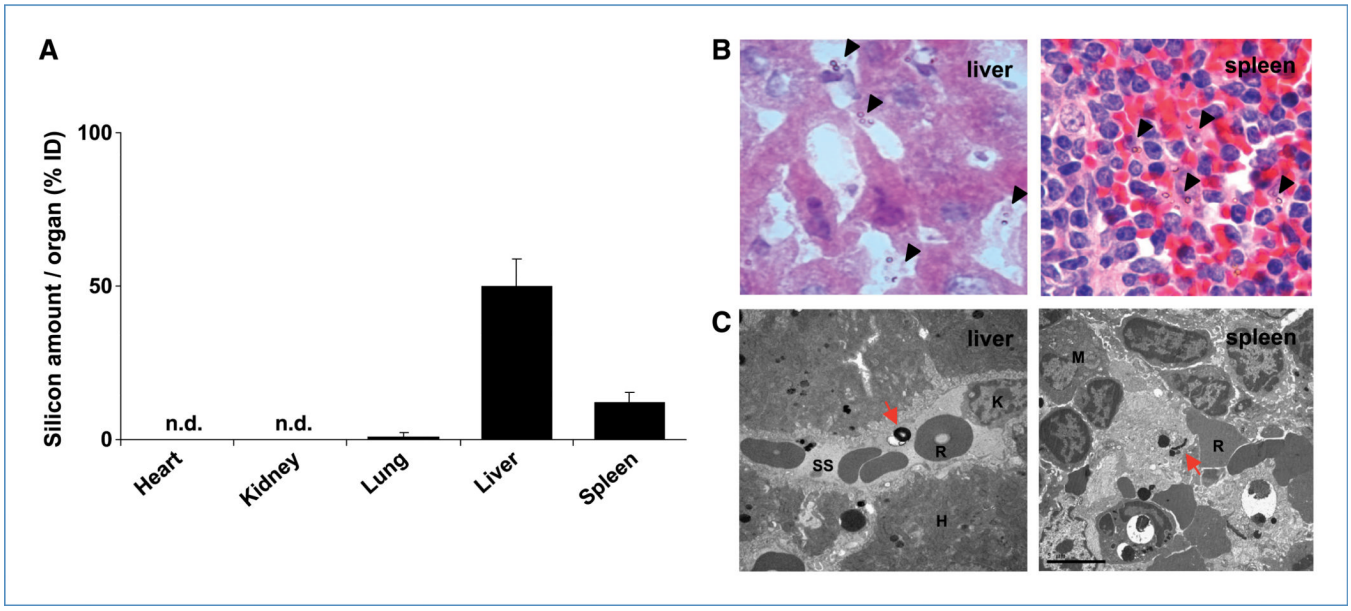

Figure 5.

Biodistribution of S1MP. A, silicon content analysis of organs isolated from mice (n = 6) following i.v. injection of S1MP-EphA2-siRNA-DOPC. The major organs including heart, lung, liver, kidney, and spleen were harvested 4 h after the i.v. injection. Silicon amounts were measured by inductively coupled plasma atomic emission spectroscopy and expressed as % of injected dose per organ (% ID). n.d., not detectable. B, H&E staining of the liver and spleen sections. The liver and spleen were harvested from the mice injected with S1MP-EphA2-siRNA-DOPC and fixed with formalin. Five-micrometer paraffin sections were stained with H&E to identify the localization of S1MP in the organs. Arrows, S1MP (final magnification, ×1,000). C, transmission electron microscopic images of S1MP in the liver and spleen. S1MP remained within the sinusoidal space in the liver (red arrow). K, Kupffer cell; R, RBC; SS, sinusoidal space; H, hepatocyte; M, macrophage (original magnification, ×10,000).

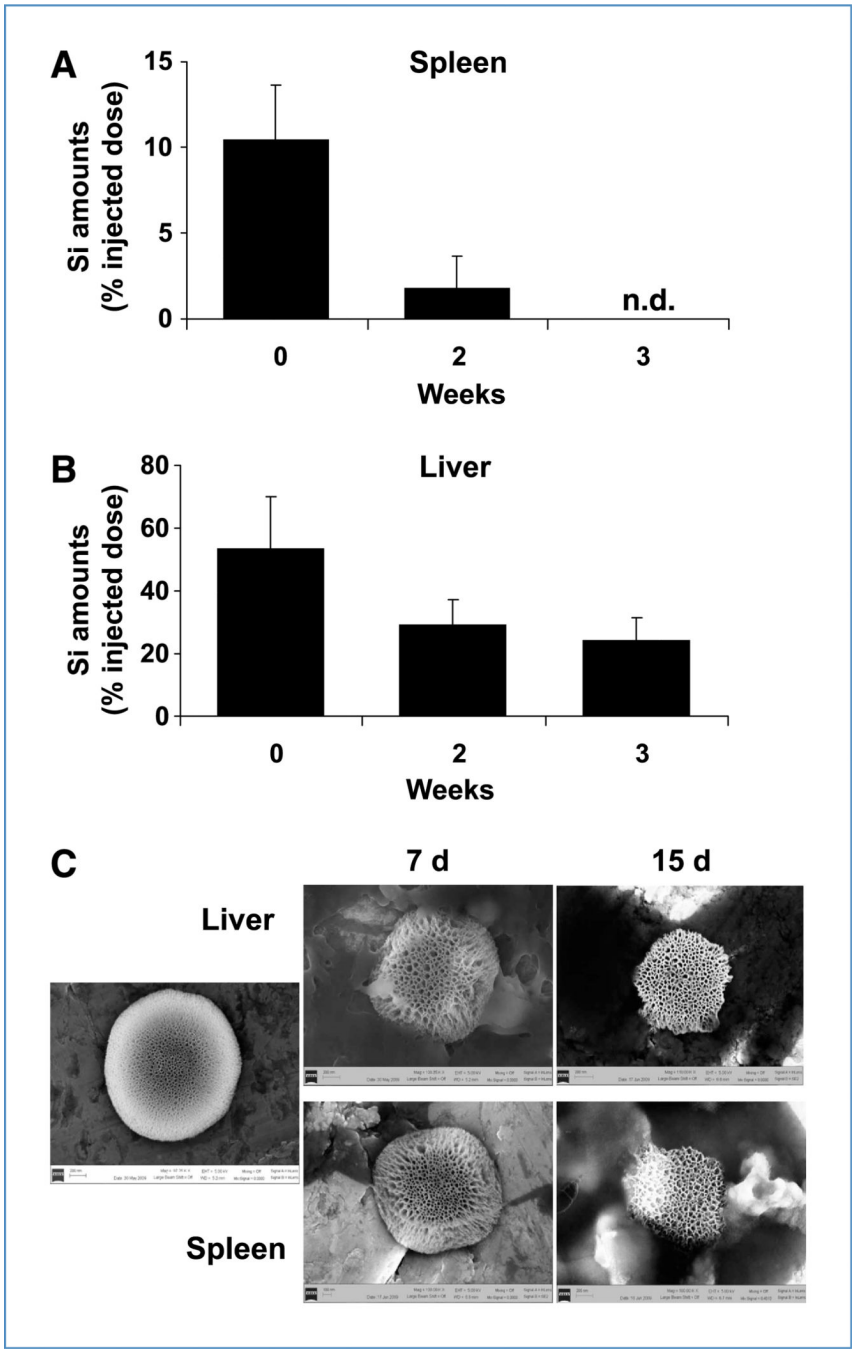

Figure 6.

Biodegradation of S1MP. The mice (n = 5) were injected with S1MP-Alexa555-siRNA-DOPC and the liver and spleen were harvested at indicated time points. The organs were processed for silicon contents analysis and SEM images. A and B, inductively coupled plasma analysis was performed to determine the silicon contents in the liver and spleen at different time points. Silicon (Si) amounts were expressed as % of injected dose per organs (% ID). C, the S1MPs were isolated from the liver and spleen homogenates and further cleaned by sonication for SEM analysis. SEM images show time-dependent biodegradation of S1MP in the liver and spleen at day 7 and 15. Original magnification, ×50,000).